

PROPERTIES OF THE BACKGROUND OF EPIC ONBOARD XMM-NEWTON

H. Katayama¹, I. Takahashi², Y. Ikebe³, K. Matsushita³, Y. Tanaka³, and M. Freyberg³

¹Department of Earth and Space Science, Graduate School of Science, Osaka University, 1-1 Machikaneyama, Toyonaka, 560-0043 Osaka, Japan

²Department of Physics, University of Tokyo, 7-3-1 Hongo, Bunkyo-ku, 113-0033 Tokyo, Japan

³Max Planck Institut für Extraterrestrische Physik, Postfach 1312, 85741 Garching, Germany

ABSTRACT

Understanding a background is crucial in particular for a study of low surface brightness objects. In order to establish the background subtraction method, we have studied properties of the EPIC background.

Count rates of the background vary violently by two order of magnitude at the maximum, while during the most quiet period, these are stable within 8 % at a 1σ level. The overall spectrum is dominated by particle events above 5 keV, and its spatial variation is also found.

The long-term variation of the background is also investigated with CAL CLOSED data, which is the data of calibration source with filter closed. The average background count rate decreased by 20 % from March 2000 to January 2001, but it regained in February 2001.

For the modeling of the background spectrum, we investigate correlations between the 2-10 keV count rate and some characteristic parameters. The PN background shows a good correlation with some parameters. On the other hands, the MOS background does not shows a clear correlation. Further investigation is needed for the MOS background.

Our final goal is to establish a method to predict the background, for which these results will be reflected in the background generator.

Key words: Missions: XMM-Newton – background

1. DATA AND SCREENING

In order to study properties of the background, we used data from Science PV phase data operated in the full frame mode with thin filter. All the data are shown in table 1 and table 2. The number of data sets is 8 for PN and 7 for MOS.

Figure 1 shows a light curve of PN from one of the Lockman hole observations. In order to exclude the flare events, time periods where the count rate deviates from the mean value during quiescent periods by $\pm 2\sigma$ are excluded. Celestial sources and noisy columns are also excluded from the data. The average exposure time thus remained after excluding the flare events is 18 ks for PN and 26 ks for MOS.

Obs ID	Exposure	Object
0063_0123100201_PNS001	11411	MS0737.9+7441
0070_0123700101_PNS003	27695	Lockman Hole
0071_0123700201_PNS003	21009	Lockman Hole
0073_0123700401_PNS003	9977	Lockman Hole
0078_0124100101_PNS003	21403	RXJ0720.4-3125
0081_0123701001_PNS003	17569	Lockman Hole
0082_0124900101_PNS003	17665	MS1229.2+6430
0181_0098810101_PNS003	18529	WW Hor

Table 1. PN data summary

Obs ID	Exposure	Object
0070_0123700101_M1S001	30552	Lockman Hole
0071_0123700201_M1S001	33269	Lockman Hole
0078_0124100101_M1S001	28794	RXJ0720.4-3125
0081_0123701001_M1S001	21358	Lockman Hole
0100_0123701001_M1S001	21258	Lockman Hole
0071_0123700201_M2S002	26465	Lockman Hole
0181_0098810101_M2S002	21785	WW Hor

Table 2. MOS data summary

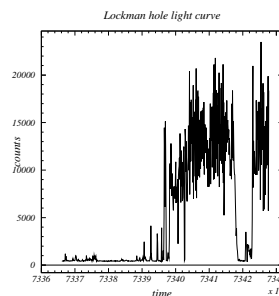


Figure 1. Light curve of Lockman hole observation.

2. SPECTRUM OF BACKGROUND

Figure 2 shows average background spectra of XMM EPIC. Internal backgrounds which are taken with the filter wheel in the closed position are also displayed in the same figure. The prominent features of the PN background spectrum are Al-K, Ni-K, Cu-K, and Zn-K lines. Two line features of the MOS background spectrum are Al-K and Si-K lines. The overall spectrum is dominated by particle events above 5 keV.

Background spectra from individual observations are compared in figure 3 (Top). Figure 3 (Bottom) shows their ratio to the average spectrum. The fluctuation of spectra is within 8 % at a 1σ level.

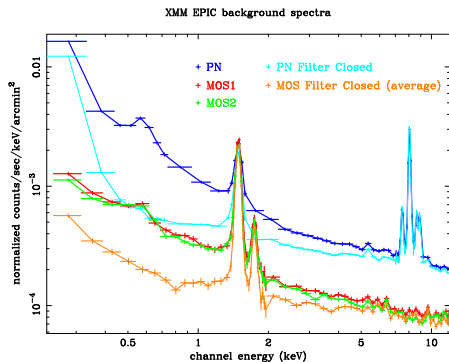


Figure 2. Average background spectra of XMM EPIC. Internal backgrounds (Filter closed) are also displayed.

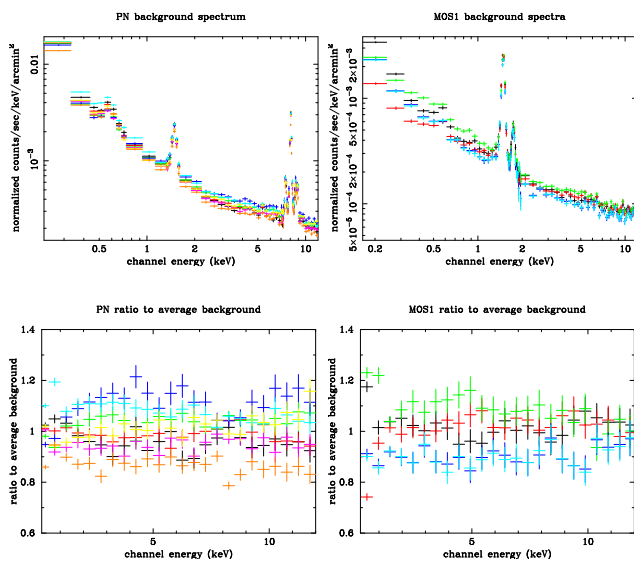


Figure 3. (Top) All background spectra of individual observations. Right is PN background spectra and Left is MOS1. (Bottom) Ratio to the average background spectrum. Colors are corresponding to individual observation of the top figure.

3. SPATIAL DISTRIBUTION OF BACKGROUND

3.1. AVERAGE SPATIAL DISTRIBUTION

Figure 4 displays the average spatial distribution of the background in different energy bands. The size of the FOV for PN and MOS is 15' and 14' radius, respectively. In the outside of the FOV, no sky X-ray is supposed to be detected, and the gap in the count rate profile is prominent in soft energy bands. Vignetting effect of telescope is also

seen in the lower energy band, while the continuum emission in the higher energy band makes almost flat spatial distribution. Fluorescent lines show peculiar profiles (see XMM User's hand book and Freyberg (2001) in this contribution).

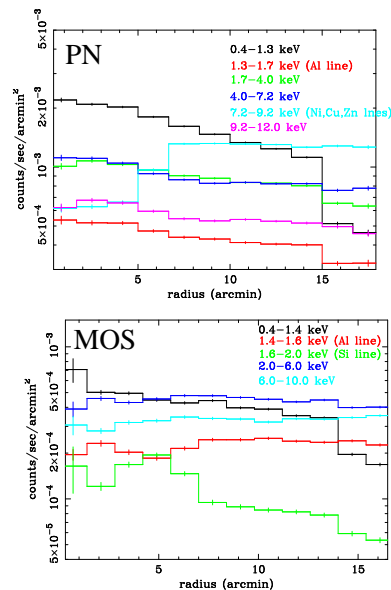


Figure 4. (Top) Average spatial distribution of the PN background. (Bottom) Average spatial distribution of the MOS1 background.

3.2. CORRELATIONS OF COUNT RATE

Figure 5 and figure 6 display the correlations of count rate between the region of outside of FOV and inside of FOV in different energy bands. Red, green, and blue crosses indicate the data sets of 0-5', 5-10', and 10-15', respectively. The PN data set shows a good correlation in the energy band of 1.7-4.0 keV and 4.0-7.2 keV. Thus, this result represents that the shape of background distribution does not change in these energy bands. This also implies that the count rate of outside of FOV is available for background monitoring. On the other hands, The MOS data set does not show any clear correlation. As we examined only five data sets for MOS1, further investigation is needed for MOS.

4. LONG-TERM VARIATION OF BACKGROUND

In order to investigate the long-term variation of the PN background, we used CAL CLOSED data, which is calibration source data with filter closed. Figure 7 (Left) displays the spectra of the Lockman hole, filter closed, and CAL CLOSED data. The 7.0-13.0 keV band is free from events by the calibration source, and its count rate can be usable for monitoring the background count rate.

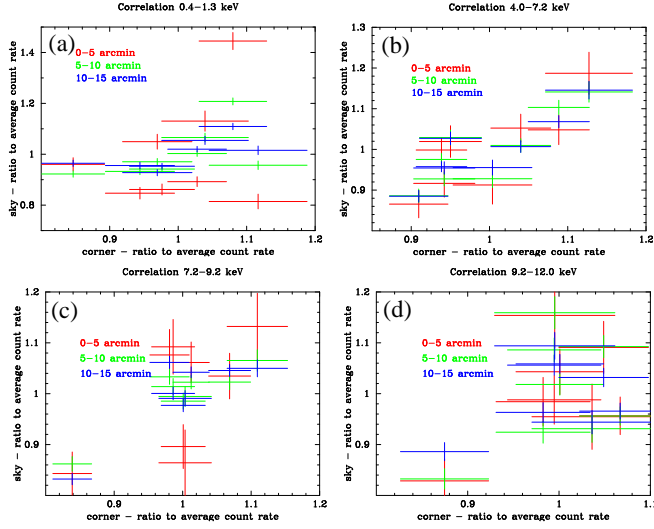


Figure 5. Correlations of PN count rate between the region of outside of FOV and within FOV in different energy bands. (a) 0.4–1.3 keV (b) 4.0–7.2 keV (c) 7.2–9.2 keV (d) 9.2–12.0 keV.

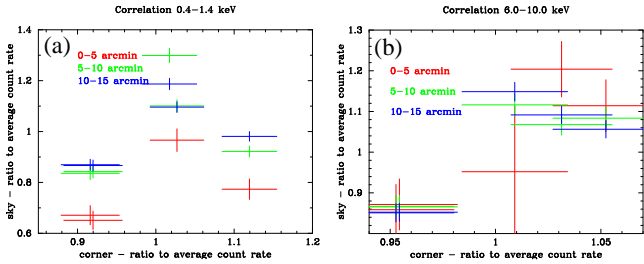


Figure 6. Correlations of MOS count rate between the region of outside of FOV and inside FOV in different energy bands. (a) 0.4–1.4 keV (b) 6.0–10.0 keV.

The top panel of figure 7 (Right) displays the long-term light curve in the 7.8–8.3 keV and 10.0–13.0 keV band derived from the CAL CLOSED data. The average background count rate decreased by 20 % from March 2000 to January 2001, however, it regained in February 2001. This long term variation is most probably related to the solar activity. One could see the similar trend in the variation of the number of sunspots shown in the bottom panel of figure 7 (Right).

5. PARAMETERS FOR BACKGROUND MODELING

In order to obtain the parameter for background modeling, we investigated the correlations between characteristic parameters and the 2–10 keV count rate.

1 Number of discarded columns

For PN, the column that detects an event above upper energy threshold and its neighbor columns are removed from the data as a background. This is called MIP rejection. As most of these MIP events are cosmic-ray

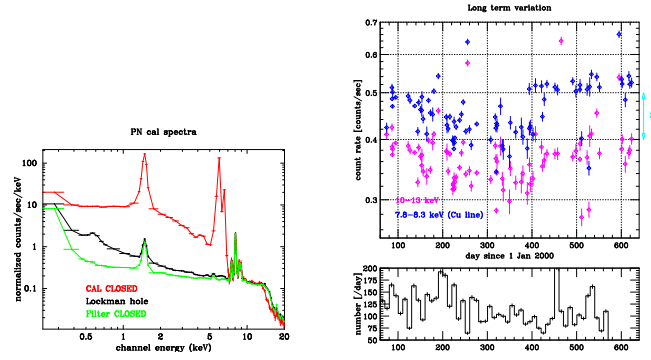


Figure 7. (Right) Spectra of the Lockman hole (Black), filter closed (Green), and CAL CLOSED data (Red). (Left) Long-term variation of the 7.8–8.3 keV and 10.0–13.0 keV count rate. The horizontal axis is the day since January 2000. The number of sunspots in the same term is also displayed in the bottom panel.

events, the number of columns that are discarded by MIP rejection is expected to be related to the remaining background count rate.

Figure 8 shows the relation between the 2–10 keV count rates and the number of discarded columns. There is no clear correlation between these two parameters. This might be because the energy spectrum of particles changes temporally. MIP events are attributed to all particles of which energy is above a certain extent. The population of such particles is very large. On the other hands, the 2–10keV background, in particular the continuum, is attributed to a portion of the whole particles that have a certain configuration of the energy and the incident direction. Therefore, the 2–10keV background count rate would fluctuate largely by the temporal change of the particle energy spectrum.

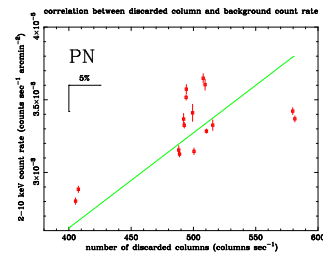


Figure 8. Correlation between the number of discarded columns and the 2–10 keV count rate.

2 Count rate of 10–12 keV

For many sources, emissions above 10 keV are negligibly small compared with the background. Thus, the count rate above 10 keV could be usable for the background modeling.

In figure 9, the background count rates in 10–12 keV are plotted against those in 2–10 keV. The PN data

set shows a good correlation, while the MOS data set does not show a clear correlation.

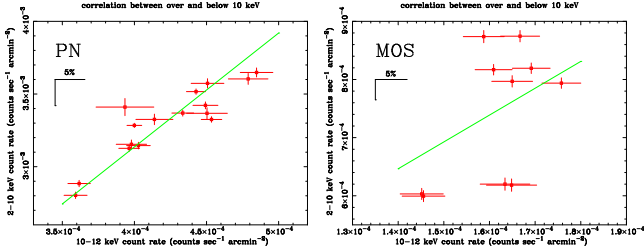


Figure 9. correlations between the 10–12 keV count rate and the 2–10 keV count rate.

3 Count rate of outside of FOV

Figure 10 displays the 2–10 keV count rate detected outside of FOV vs. that in FOV. The PN data set shows a good correlation.

The good correlation seen for the PN data can be usable for monitoring the background. In order to examine the efficacy, each spectrum shown in figure 3 is renormalized so that the corresponding count rate of outside of FOV becomes the same as that of the average value. Figure 11 shows the fluctuations (standard deviations of 1σ) of original spectra and corrected spectra. The variation of PN background spectra decreases from 8% to 3% in the 2–7 keV band.

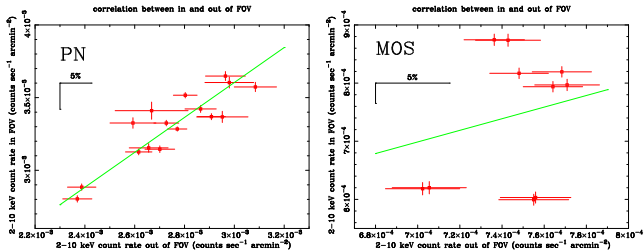


Figure 10. Correlations between the 2–10 keV count rate of outside of FOV and that of in FOV.

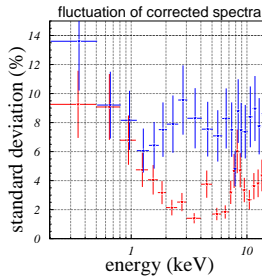


Figure 11. Standard deviations of PN background spectra. Blue data are original spectra and Red data are spectra corrected by count rates of outside of FOV. The variation decreases from 8% to 3% in the 2–7 keV band.

6. COMPARISON WITH ASCA AND CHANDRA

Finally, we show the comparison of the background spectra among different X-ray CCDs onboard XMM, ASCA, and Chandra. The background spectrum of ASCA SIS is obtained from a blank sky data. The Chandra ACIS-S and ACIS-I data used here are also taken from blank sky observations compiled by Markevitch (2001).

The top panel of figure 12 shows the background spectra normalized by CCD area, which thus represents the background count rate per unit area on the focal plane. As these spectra include CXB component, a direct comparison on the particle event flux is meaningful only above about 5keV. The difference of the background count rates among different instruments should be explained by the cosmic-ray-particle flux depending on the satellite orbit, and the sensitivity of the CCDs, which is governed by the thickness of the depletion layer and other structure (e.g. front-illuminated or back-illuminated).

In the bottom panel of figure 12, each spectrum is normalized by the effective area of the X-ray telescope plus CCD and by the solid angle of the FOV. Thus, it represents a surface brightness of the background. ASCA SIS is the most sensitive for faint diffuse X-ray sources.

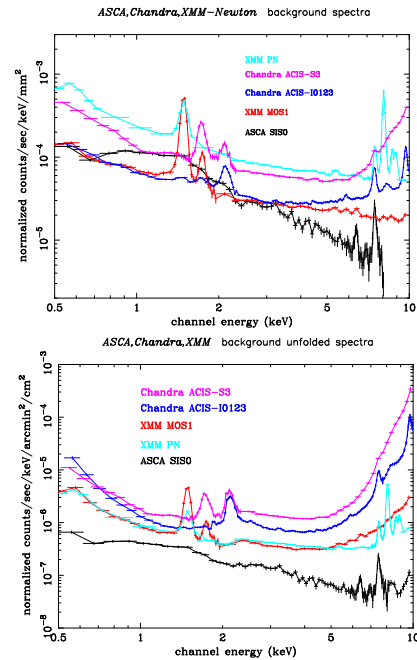


Figure 12. (Top) XMM, Chandra, and ASCA background spectra normalized by CCD area. (Bottom) XMM, Chandra, and ASCA background spectra normalized by effective area.

REFERENCES

Ehle, M., Breittellner, M., Dahlem, M. et al. 2001, XMM-Newton Users' Handbook, XMM-Newton SOC Team

Markevitch, M. 2001, ACIS background, ACIS Team

Freyberg, M. 2001, in Symp. New Visions of the X-ray Universe in the XMM-Newton and Chandra Era (ESA SP-488; Noordwijk: ESA),